

# Fine-structure electron-impact excitation of $\text{Ne}^+$ and $\text{Ne}^{2+}$ for low temperature astrophysical plasmas

Qianxia Wang<sup>1</sup>, S. D. Loch<sup>1,\*</sup>, Y. Li<sup>1</sup>, M. S. Pindzola<sup>1</sup>, R. S. Cumbee<sup>2</sup>, P. C. Stancil<sup>2</sup>, B. M. McLaughlin<sup>3</sup>, and C. P. Ballance<sup>3†</sup>

<sup>1</sup>*Department of Physics, Auburn University, AL 36849, USA*

<sup>2</sup>*Department of Physics and Astronomy and Center for Simulational Physics, University of Georgia, GA 30602, USA and*

<sup>3</sup>*CTAMOP, School of Mathematics and Physics, Queen's University, Belfast, Belfast BT7 1NN, UK*

(Dated: April 25, 2022)

Collision strengths for electron-impact of fine-structure level excitation within the ground term of  $\text{Ne}^+$  and  $\text{Ne}^{2+}$  are calculated using the Breit-Pauli, Intermediate Coupling Frame Transformation, and DARC  $R$ -matrix methods. Maxwellian-averaged effective collision strengths and excitation rate coefficient  $q_{ij}$  are presented for each. The application of the current calculations is to very low temperature astrophysical plasmas, thus we examine the sensitivity of the effective collision strengths down to 10 K. The use of the various theoretical methods allows us to place estimated uncertainties on the recommended effective collision strengths. We also investigate the sensitivity of the collision strengths to the resonance positions and underlying atomic structure. Good agreement is found with previous  $R$ -matrix calculations at higher temperature.

PACS numbers:

## I. INTRODUCTION

Electron-impact fine-structure excitation of low charged ions is an important cooling mechanism in most interstellar environments, especially in regions with significant ionization fraction where electron-impact excitation is a strong populating mechanism for the excited states. The lines from these fine-structure transitions can be observed from the infrared (IR) to the submillimeter (submm) by a range of telescopes (e.g., the *Spitzer Space Telescope*, the Stratospheric Observatory for Infrared Astronomy (SOFIA), the *Herschel Space Observatory*, the Atacama Large Millimeter Array (ALMA), etc.). Further, fine-structure excitation due to electron-impact is an important diagnostic tool for the density, pressure, temperature, and/or ambient radiation field, if sufficiently accurate rate coefficients can be obtained. Electron impact fine-structure excitation has been studied fairly extensively for many ions over the past few decades (Pradhan 1974; Butler & Mendoza 1984; Johnson et al. 1987; Saraph & Tully 1994; Griffin et al. 2001; Colgan et al. 2003; Berrington et al. 2005; Witthoef et al. 2007; Munoz Burgos et al. 2009; Ludlow et al. 2011; Malespin et al. 2011; McLaughlin et al. 2011; Wu et al. 2012; Abdel-Naby et al. 2013; Abdel-Naby et al. 2015). However, almost all of these studies have primarily focused on high energies/high temperatures relevant to collisionally-ionized plasmas and some of the existing fine-structure excitation rate coefficients in current astrophysical codes are still based on a simple model developed by Bahcall & Wolf (1968), which may lead to inaccurate

results.

For the plasmas of importance in this paper, we require rate coefficients down to approximately 10 K, appreciating that achieving the accuracy in the underlying cross section at this temperature is difficult. Therefore it is important for astrophysical models that collisional calculations are performed down to lower energies and that the associated rate coefficients are updated.

The fine-structure line emissions, Ne II and Ne III, due to electron-impact excitation of  $\text{Ne}^+$  and  $\text{Ne}^{2+}$ , respectively, are observed in the IR and known to be very important for probing H II regions. Previous work (Glassgold et al. 2007; Meijerink et al. 2008) has proposed that Ne II and Ne III fine-structure lines are appropriate to serve as diagnostics of the source of an evaporative flow, as well as of signatures of X-ray irradiation, so-called X-ray dominated regions (XDRs). This is because hard X-rays have sufficient energy to generate multiple ionization states of neon which can then be collisionally excited. The rate coefficients used in most applications are based on the approximations of Bahcall & Wolf (1968). However,  $R$ -matrix methods have been available for these and neighboring ion stages of Ne. Specifically, collision strengths for the  $1s^2 2s^2 2p^5$  ( $^2P_{3/2}^0$ ) - ( $^2P_{1/2}^0$ ) transition of  $\text{Ne}^+$  have been calculated using a  $R$ -matrix method via the jj omega (JAJOM) approach (Johnson & Kingston 1987; Saraph & Tully 1994). The collision strengths of the transitions among levels of the lowest configurations for  $\text{Ne}^{2+}$  were evaluated by Pradhan (1974) and Butler & Mendoza (1984), also with an  $R$ -matrix method. McLaughlin et al. (2000, 2002) extended this approach to a large configuration-interaction representation of the target, supplemented by a few extra pseudo-orbitals to improve the target description further. Here, we have re-investigated these two Ne ions for several reasons.

Previous work has focused primarily on higher

\*Electronic address: loch@physics.auburn.edu

†Electronic address: C.Ballance@qub.ac.uk

electron-impact energies than considered here with only a few of their Maxwellian averaged effective collision strengths going below 800 K. This leads naturally to the second focus of the paper, which is the exploration of uncertainty in the rate coefficients at very low temperatures. To this end, three different theoretical level-resolved  $R$ -matrix approaches have been applied: the Intermediate Coupling Frame Transformation (ICFT) approach (Griffin et al. 1998), the Breit-Pauli (BP) approximation (Berrington et al. 1987), and the fully relativistic Dirac method (Norrington et al. 1981; Dyaal et al. 1989). Obstinately, if the underlying electronic structure adopted in each approach was exactly the same there would be little expectation of differences in the collision strengths. However, with the use of different atomic structure codes and the choices made in their use, this invariably leads to small differences in  $A$ -values and subsequently, dynamical quantities such as collision strengths.

Thus, we are interested in the sensitivity of the effective collision strengths to the threshold energy position, the target wave-functions, resonance positions, and anything that can affect the background cross section. We appreciate that the height and position of a single resonance can dramatically affect the results at these temperatures. We shall explore the variation in results to threshold energy and resonance positions by calculating collision strengths where the target energies have been shifted (or not) to NIST energies (Kramida et al. 2015). Furthermore, we explore the sensitivity of the target wave-function via different target expansions within the BP  $R$ -matrix, ICFT  $R$ -matrix, and DARC  $R$ -matrix methods. After investigating the differences between all calculated effective collision strengths for the same transition, we recommend one based upon our findings.

We focus on excitation at low temperatures in this paper. So for  $\text{Ne}^+$ , only rates for the transition between the two lowest levels  $1s^2 2s^2 2p^5 ({}^2P_{3/2}^0) - ({}^2P_{1/2}^0)$  are presented. Also, the transitions between the three lowest fine-structure levels of  $\text{Ne}^{2+}$  (see energy diagram in Figure 1) are investigated here.

The rest of this article is organized as follows. In Sec. 2, we describe the three theoretical methods used in this paper. The calculated results, target energies, Einstein  $A$  coefficients, collision strengths, effective collision strengths and excitation rate coefficients for  $\text{Ne}^+$  and  $\text{Ne}^{2+}$  will be discussed in Sec. 3. Sec. 4 provides a summary of the results.

## II. THEORY

Level-resolved electron-impact excitation calculations using  $R$ -matrix theory, employs a similar formalism whether semi-relativistic or relativistic implementations are used.  $\text{Ne}^+$  and  $\text{Ne}^{2+}$  are not highly charged, therefore both semi-relativistic and fully relativistic methods are equally applicable. The main differences arise from the choices made in the determination of the target orbitals.

The atomic structure code AUTOSTRUCTURE (Bannell 1986) generates non-relativistic orbitals whereas the General Relativistic Atomic Structure Package (GRASP; Dyaal et al. 1989) formulates and diagonalizes a Dirac-Coulomb Hamiltonian to produce the relativistic orbitals. The former is used in the BP/ICFT (Berrington et al. 1995) collisional calculations and the latter in the Dirac Atomic  $R$ -matrix Code (DARC; Chang 1975; Norrington & Grant 1981) calculations.

The BP  $R$ -matrix method is a set of parallel codes developed from modified serial versions of the RMATRIX I codes (Berrington et al. 1995). Both the BP and ICFT models recouple underlying  $LS$  coupling calculations, the former transforms several  $LS$ -resolved Hamiltonians into a  $jK$ -coupled Hamiltonian, pre-diagonalisation, as opposed to the ICFT approach that transforms unphysical  $LS$ -resolved  $K$ -matrices into level-resolved collision strengths. In general there has been very good agreement between the ICFT and BP  $R$ -matrix methods (Griffin et al. 1998; Munoz Burgos et al. 2009).

The implementation of various flavours of  $R$ -matrix theory are used in this study. The review book of Burke (Burke 2011) provides an excellent overview of non-relativistic ( $LS$  coupling), semi-relativistic (BP/ICFT) and relativistic (DARC) electron-impact excitation. The comparison of BP and ICFT results benefits from the use of a completely consistent atomic structure as opposed to multiconfiguration Dirac-Fock (MCDF) results from GRASP, though in all cases every effort has been made to optimize the orbitals on the fine-structure levels of the ground term. The DARC calculation employs relativistic orbitals from the initial atomic structure calculations throughout the remainder of the computation. It should be restated that low temperature astrophysical constraints on both our Ne systems means we are pursuing only transitions between the fine-structure levels of the ground term, and that any excited states are included for the main purpose of improving the energy levels of those low-lying states through configuration interaction. Given that the energy separation between the ground state  $n = 2$  and the excited  $n = 3$  levels for either  $\text{Ne}^+$  or  $\text{Ne}^{2+}$  exceeds 2 Ryd., it is unlikely that Rydberg states attached to the  $n = 3$  levels would perturb our  $n = 2$  results.

## III. CALCULATION DETAILS

### A. Target state calculation

Given the low temperature focus of this paper, only small scale calculations are required for the fine-structure transitions within the ground term. Furthermore, we would like to explore the variation of our results in relation to various configuration-interaction (CI) expansions. Thus, we consider both a small and larger CI expansion for  $\text{Ne}^+$  and  $\text{Ne}^{2+}$ , with the configurations described in Table I. The models are referred to as BP  $n = 2$ , DARC

$n = 2$ , BP  $n = 3$ , and DARC  $n = 3$ .

For the ICFT  $R$ -matrix method, we only perform calculations for one target expansion, and the included configurations are the same as BP/DARC  $n = 3$ . This will be used to explore the difference between the BP and ICFT methods.

We also performed optimized BP and ICFT calculations, using orbital scaling parameters to improve the target structure. We use the Thomas-Fermi-Dirac-Amaldi potential, with appropriate scaling parameters. The orbital scaling parameters are  $\lambda_{1s}=1.0$ ,  $\lambda_{2s}=1.3$ ,  $\lambda_{2p}=1.09$ ,  $\lambda_{3s}=1.13$ ,  $\lambda_{3p}=1.15$ ,  $\lambda_{3d}=1.11$  for  $\text{Ne}^{2+}$ , taken from McLaughlin et al. (2011). We refer to these calculations as BP(op)  $n = 2/n = 3$  and ICFT(op)  $n = 3$  in the following sections.

### B. Scattering calculation

Here we only present details specific to the current  $R$ -matrix calculations. The radius of the  $R$ -matrix sphere used for  $\text{Ne}^+$  is 5.40 a.u. for DARC  $n = 2$ , 19.83 a.u. for DARC  $n = 3$ , 5.87 a.u. for BP  $n = 2$ , and 21.60 a.u. for BP  $n = 3$ . For the ion  $\text{Ne}^{2+}$ , the radius of the  $R$ -matrix sphere is 4.89 a. u. for DARC  $n = 2$ , 13.28 a.u. for DARC  $n = 3$ , 5.24 a.u. for BP  $n = 2$ , 14.35 a.u. for BP  $n = 3$ , 4.91 a.u. for BP(op)  $n = 2$ , 14.22 a.u. for BP (op)  $n = 3$ , and 14.22 a.u. for ICFT(op)  $n = 3$ . 20 continuum basis orbitals for each angular momentum are chosen for BP/BP(op)/DARC  $n = 2$  for both  $\text{Ne}^+$  and  $\text{Ne}^{2+}$ , which is more than sufficient to converge the results for the low temperature calculations. All of our models include partial waves from  $J = 0$  to 10, which is more than sufficient to converge the cross sections for the energy region for our calculations. An energy mesh of  $2.5 \times 10^{-6}$  Rydbergs for  $\text{Ne}^+$  and  $3.125 \times 10^{-6}$  Rydbergs for  $\text{Ne}^{2+}$  ensured resonances were resolved, particularly for the lowest temperatures of subsequent effective collision strengths. We calculate collision strengths up to 0.107 Ryd. for  $\text{Ne}^+$  and 0.1658 Ryd. for  $\text{Ne}^{2+}$ , and effective collision strengths from 10-2000 K for both ions. All these parameters are listed in Table II

### C. Effective collision strength calculation

The effective collision strength (Seaton 1953; Eissner et al. 1969) can be calculated from the collision strengths via:

$$\Upsilon_{ij} = \int_0^\infty \Omega_{ij} \exp\left(\frac{-\epsilon_j}{kT_e}\right) d\left(\frac{\epsilon_j}{kT_e}\right), \quad (1)$$

where  $\Omega_{ij}$  is the collision strength for the transition from level  $i$  to  $j$ ,  $\epsilon_j$  is the energy of the scattered electron,  $T_e$  the electron temperature, and  $k$  Boltzmann's constant.

The Maxwellian excitation rate coefficient  $q_{ij}$  is the coefficient used widely in astrophysics. The relationship

between  $q_{ij}$  and  $\Upsilon_{ij}$  is

$$q_{ij} = 2\sqrt{\pi}\alpha c a_0^2 \left(\frac{I_H}{kT_e}\right)^{1/2} \frac{1}{\omega_i} e^{-\frac{\Delta E_{ij}}{kT_e}} \Upsilon_{ij}, \quad (2)$$

where  $\alpha$  is the fine-structure constant,  $c$  the speed of light,  $a_0$  the Bohr radius,  $I_H$  the hydrogen ionization potential,  $\Delta E_{ij}$  the energy difference in the fine-structure levels, and  $\omega_i$  the degeneracy in the lower level. Compared with  $q_{ij}(T_e)$ ,  $\Upsilon_{ij}(T_e)$  is a smoother function and can be more accurately interpolated.

## IV. RESULTS AND DISCUSSION

Astrophysical plasma modelers who study IR/submm observations of low temperature plasmas, such as the interstellar medium, require atomic rate coefficients down to temperatures as low as 10 K. This will place very stringent tests on the accuracy of the atomic structure and collisional calculations. The excitation rate coefficients will be very sensitive to small changes in the atomic structure. As a result, the structure will impact the rate coefficients through changes in the threshold energy, resonance strengths and positions, and changes in the background cross section. For this reason, we have performed a range of calculations using different methods (BP  $n = 2$ , DARC  $n = 2$ , BP  $n = 3$ , DARC  $n = 3$ , BP(op)  $n = 3$ ). These will be used to explore the variation of the effective collision strengths, particularly at low temperatures. The purpose of including the  $n = 3$  configurations is to improve the energies and transition probabilities for the levels within the ground term.

### A. Bound-state energies and radiative rates for $\text{Ne}^+$ and $\text{Ne}^{2+}$

Our recommended dataset shall be the model that minimizes the difference between that calculation and the NIST A-values and level energies (Kramida et al. 2015). The results are shown in Tables III and IV. The percent error shown is calculated by  $\frac{x-x_{\text{NIST}}}{x_{\text{NIST}}} \times 100\%$  with the NIST data providing the accepted values.

The BP/DARC  $n = 2$  and  $n = 3$  target expansions give rise to 3 and 108 levels for  $\text{Ne}^+$ , and 10 and 226 levels for  $\text{Ne}^{2+}$ . The energies for the levels within the ground term are presented in Table III and the associated A-values in Table IV. In general, the percent errors show that the agreement between theoretical and NIST values is reasonable. The  $n = 3$  target expansion results in marginally better energies for both ions and different  $R$ -matrix methods compared to the  $n = 2$  expansion. For  $\text{Ne}^+$ , the average percentage error for the BP  $n = 2$ , BP  $n = 3$ , DARC  $n = 2$ , and DRAC  $n = 3$  target expansions are 1.41%, 0.96%, 3.6% and 0.42%, respectively. While for  $\text{Ne}^{2+}$ , the corresponding average percent errors for target energies are 8.13%, 6.95%, 3.72% and 3.33%.

Optimized BP calculations are also performed for  $\text{Ne}^{2+}$ , giving average percentage errors of 3.34% for BP(op)  $n = 2$  and 3.20% for BP(op)  $n = 3$ . The DARC  $R$ -matrix method produces better energies than the BP  $R$ -matrix method for  $\text{Ne}^{2+}$  for both  $n = 2$  and  $n = 3$ . The optimized BP calculation for  $\text{Ne}^{2+}$  dramatically increases the accuracy of the energies.

Table IV presents the comparison of Einstein A coefficients for both the  $\text{Ne}^+$  and  $\text{Ne}^{2+}$  transitions. In both cases, the DARC  $n = 2$  calculations produce the closest agreement with NIST values. The remainder of the dataset shall be used to gauge the variation between the different calculations. The accuracy of the Einstein A coefficient is not only related to the precision of the target energies, but also depends on the reliability of the target wave-functions. The optimized BP  $n = 3$  calculation does give better target energies and A-values compared with the BP(op)  $n = 2$ , showing an improvement with CI expansion. This trend is not reflected in the DARC results, see Tables III and IV. We conclude that our recommended dataset is the DARC  $n = 2$  calculation which has the most accurate target energies and A-values, and will provide the most accurate collision strengths, effective collision strengths and excitation rate coefficients. We also investigated the differences between an ICFT(op) and the BP(op) calculation for  $\text{Ne}^{2+}$  using the same structure, noticing no differences in the effective collision strengths.

### B. Collision strengths and effective collision strengths for $\text{Ne}^+$ and $\text{Ne}^{2+}$

To our knowledge, there are no experimental results for the collision strengths for transitions within the ground complex for either of these ion stages. Our goal is to determine the variation in effective collision strengths between our best models as we progress to the very low temperatures required by the astrophysical applications. We have adopted two different approaches to calculating meaningful representative percent differences in our work.

In the first approach we calculate a percentage uncertainty on the effective collision strengths simply using the standard deviation of our three most accurate models as determined from the accuracy of the energy levels and the associated A-values, given by

$$\% \Delta = \frac{\sigma(\bar{x}_{best})}{x_i} \times 100\% \quad (3)$$

where  $\sigma(\bar{x}_{best})$  is the standard deviation. Secondly, we obtain a percent difference comparing results from our semi-relativistic and fully-relativistic  $R$ -matrix methods employing exactly the same set of non-relativistic target configurations. In this case, the percentage difference is calculated by the formula  $\frac{x_1 - x_2}{(x_1 + x_2)/2} \times 100\%$ .

Figures 2 – 5 illustrate the collision strengths and effective collision strengths for the fine-structure transitions of

both  $\text{Ne}^+$  and  $\text{Ne}^{2+}$ , using the different  $R$ -matrix methods. Figures 6 – 8 explore the effects of shifting the target threshold energies to NIST values.

Sampling a range of calculations allows us to more objectively explore the variation of collision strength in regards to the size of the different CI expansions. As stated earlier, the sizeable energy separation between the  $n = 2$  and  $n = 3$  levels precludes the possibility of interloping resonances attached to the  $n = 3$  levels perturbing the cross sections from transitions amongst the  $n = 2$  levels. The influence of resonance contributions to effective collision strengths is only expected for the case of  $\text{Ne}^{2+}$  due the  $2p^4$  subshell supporting 3 levels within the ground state complex, whereas the resonances attached to the upper  $J = \frac{1}{2}$  levels of  $\text{Ne}^+(2p^5)$  lie in the elastic cross section of the  $\text{Ne}^+$  ground state.

Figure 2 shows collision strengths (top) and effective collision strengths (bottom) for the  $\text{Ne}^+ 2s^2 2p^5 ({}^2P_{3/2}^0) - ({}^2P_{1/2}^0)$  transition. The largest collision strengths are from the BP  $n = 2$  calculation, the next lower one is from the DARC  $n = 2$  calculation, then from BP  $n = 3$  and DARC  $n = 3$ . The DARC  $n = 2$  calculation is our recommended data set based upon A-value comparisons with the NIST database values. Furthermore, in the absence of experiment, the MCDF approach would be our recommended theoretical model. Subsequent effective collision strengths were generated from the respective collision strengths of each calculation. We note that beyond the current work, a previous large-scale BP  $R$ -matrix calculation for  $\text{Ne}^+$  has been carried out Griffin et al. (2001). However, the focus of that work was to provide a large comprehensive data set across a wide range of temperatures, but not at the very low temperatures required by our study. At 1000 and 2000 K, the DARC  $n = 2$  effective collision strengths were in best agreement with this previous work. Our effective collision strengths are 0.302 at 1000 K and 0.304 at 2000 K, compared with 0.266 and 0.286 from Griffin et al. (2001), as shown in Fig. 2, giving differences of 12.7% and 6.1%, respectively. Thus, this supports our independent conclusion that our DARC  $n = 2$  effective collision strengths should be the recommended dataset at even lower temperatures, and are tabulated in Table V.

Employing the average percentage uncertainty given by Equation (3), the  $\bar{x}_{best}$  values used to calculate the uncertainty are the BP  $n = 2$ , BP  $n = 3$ , and the DARC  $n = 2$  results, providing an uncertainty from 19.1-19.6% for our recommended DARC  $n = 2$  effective collision strengths, as shown in Figure 2.

It is also of interest to consider the differences between the DARC and BP calculations, for the cases when they both have the same configurations. The differences of the effective collision strengths between the DARC  $n = 2$  and BP  $n = 2$  are 11.3 – 12.1%, while the DARC  $n = 3$  and BP  $n = 3$  differ by 23.7 – 24.7%, which is consistent with the differences between the A-values from these calculations. We note that, perhaps counterintuitively, the DARC  $n = 3$  results drift from the recommended values,

however the explanation lies in the fact that the DARC code will endeavour to optimise all orbitals on an equal footing, when in fact we should focus only on the  $n = 2$  optimisation at the expense of the  $n = 3$  levels.

Figures 3 – 5 present the collision strengths (top) and effective collision strengths (bottom) for three different transitions of  $\text{Ne}^{2+}$ , namely, the  $(^3\text{P}_2) - (^3\text{P}_1)$  (Fig. 3),  $(^3\text{P}_1) - (^3\text{P}_0)$  (Fig. 4), and  $(^3\text{P}_2) - (^3\text{P}_0)$  (Fig. 5) transitions. For the collision strengths of the three transitions, the unoptimised BP  $n = 2$  result has the largest background, however an optimised structure aligns better with the DARC  $n = 2$  result. On the other hand, the previous calculation by McLaughlin et al. (2011), which extended down to 2000 K appears to be consistent with the DARC  $n = 3$  result. The difference between our DARC  $n=2$  and McLaughlin et al. (2011) are attributed to the fact that that our DARC  $n=2$  calculation was focused on generating accurate data only for fine structure transitions within the ground term, while McLaughlin et al. (2011) results were focused on higher temperatures and higher  $n$  shells in addition to the levels within the ground term. Overall, our recommended collision strength is that produced by the DARC  $n = 2$  calculation, based upon energy level and A-value comparisons with NIST data as discussed above.

The uncertainty in the DARC  $n = 2$  results are again provided in a similar fashion using Eq. 3 and the standard deviation of the other BP and DARC models. Values for  $\bar{x}_{best}$  for  $\text{Ne}^{2+}$  are taken from the DARC  $n = 2$ , BP(op)  $n = 2$ , and BP(op)  $n = 3$  calculations. It is interesting to note that the collision strengths from the optimised BP  $n = 2$  calculation deviate significantly from the unoptimised BP  $n = 2$  values.

Considering the effective collision strengths involving the higher excited state transitions (Figs. 4 and 5), the DARC  $n = 2$  model remains our recommended dataset, with uncertainties given by the previously applied method. The uncertainty of the effective collision strengths from the DARC  $n = 2$  calculations are 4.7 – 12.2% (Fig. 3), 3.2 – 19.8% (Fig. 4), and 5.5 – 16.2% (Fig. 5).

As we present rate coefficients at very low temperatures, we also investigated the sensitivity of the effective collision strengths to changes in the target threshold energy positions. It is expected that due to the Ryd-

berg states having high principal quantum numbers there should be a very strong correlation between the energy shift of the target level and the corresponding energy shift of the resonance attached to it.

This study was performed by comparing a BP calculation with shifts to NIST energies and a BP calculation with no shifts, in each case for  $\text{Ne}^{2+}$ . See Figs. 6 – 8 for the results. The difference between the two BP calculations (with/without energy shift) is up to 89.0% for the  $(^3\text{P}_2) - (^3\text{P}_1)$  transition, up to 38.7% for the  $(^3\text{P}_1) - (^3\text{P}_0)$ , and up to 31.8% for the  $(^3\text{P}_2) - (^3\text{P}_0)$ . The large difference in the first transition is due to the presence of near threshold resonances. Thus, to generate accurate low temperature rate coefficients it is important to shift to accurate, experimental energies, and the cases with near threshold resonances are particularly sensitive.

## V. SUMMARY

We calculated the collision strengths and effective collision strengths for  $\text{Ne}^+$  and  $\text{Ne}^{2+}$  with BP, ICFT and DARC  $R$ -matrix methods. We are interested in the rates at low temperature (10 – 2000 K), so we focus on small energies (0.007 – 0.107 Ryd. for  $\text{Ne}^+$  and 0.0058 – 0.1658 Ryd. for  $\text{Ne}^{2+}$ ) and perform small scale  $R$ -matrix calculation. After comparing the energies, the Einstein A coefficient ( $A_{ij}$ ), collision strengths ( $\Omega_{ij}$ ), effective collision strengths ( $\Upsilon_{ij}$ ) and the Maxwellian excitation rate coefficient  $q_{ij}$  we conclude that the DARC  $n = 2$  model gives rise to the most reliable collision strengths and effective collision strengths with the Einstein A coefficients generated by this method being closest to the recommended values (i.e., NIST). Further, effective collision strengths computed with the DARC  $n = 2$  approach result in rates which agree best with the existing data calculated by large-scale  $R$ -matrix methods.

## VI. ACKNOWLEDGEMENT

This work was funded under NASA grant NASA-NNX15AE47G.

- 
- [1] Abdel-Naby Sh. A., Ballance C. P., Lee T. G., Loch S. D., and Pindzola M. S., Phys. Rev. A 2013; 87: 022708.
  - [2] Abdel-Naby S A, Pindzola M S, Pearce A J, Ballance C P and Loch S D, J. Phys. B: At. Mol. Opt. Phys. 2015; 48:025203.
  - [3] Badnell N. R., J. Phys. B: At. Mol. Phys 1986; 19:3827.
  - [4] Badnell, N. R.: Comput. Phys. Commun. **182** 1528 (2011)
  - [5] Ballance, C. P., and Griffin D. C.: J. Phys. B: At. Mol. Opt. Phys. **39**, 3617 (2006)
  - [6] Ballance, C. P., Griffin, D. C., and McLaughlin, B. M.: J. Phys. B: At. Mol. Opt. Phys. **40** F327 (2007)
  - [7] Ballance, C. P., Loch S. D., Pindzola M. S., and Griffin D. C.: J. Phys. B: At. Mol. Opt. Phys. **46**, 055202 (2013)
  - [8] Berrington K. A., Ballance C. P., Griffin D C and Badnell N R, J. Phys. B: At. Mol. Opt. Phys. 2005; 38:1667.
  - [9] Berrington K. A., Burke P.G., Butler K., Seaton M.J., Storey P.J., Taylor K.T., and Yan Y., J. Phys. B 1987; 20:6379
  - [10] Butler K. and Mendoza C., Mon. Not. R. Astron. Soc.

- 1984; 208:17P.
- [11] Burke PG *R-matrix Theory of Stomic Collisions*
- [12] Burke, P. G.: *R-matrix Theory of Atomic Collisions: Application to Atomic, Molecular and Optical Processes.* (New York, USA: Springer) (2011)
- [13] Chang J J, J. Phys. B: At. Mol. Phys 1975; 8:2327.
- [14] Colgan J., Loch S. D., Pindzola M. S., Ballance C. P., and Griffin D. C., Phys. Rev. A 2003; 68:032712.
- [15] Dyal K.G., Grant I.P., Johnson C.T., Parpia F.A. and Plummer E.P., Comput. Phys. Commun. 1989; 55:425.
- [16] Dyal, K. G., Grant, I. P., Johnson, C. T., and Plummer, E. P.: *GRASP: A general-purpose relativistic atomic structure program.* *Comput. Phys. Commun.* **55** 425 (1989)
- [17] Eissner W, Martins P de A P, Nussbaumer H, Saraph H E and Seaton M J, Mon. Not. R. Astron. Soc. 1969; 146:63.
- [18] Glassgold A. E., Najita J. R. and Igea J. ApJ 2007; 656:515.
- [19] Grant, I. P.: *Quantum Theory of Atoms and Molecules: Theory and Computation* (New York, USA: Springer) (2007)
- [20] Griffin D. C., Mitnik D. M. and Badnell N. R., J. Phys. B 2001; 34:4401.
- [21] Griffin D C, Badnell N R and Pindzola M S, J. Phys. B: At. Mol. Phys 1998; 31:3713.
- [22] Johnson C. T. and Kingston A. E., J. Phys. B: At. Mol. Phys. 1987; 20:5757.
- [23] Berrington, K., Werner B. Eissner and Patrick H. Norringtona, comput. Phys. Commun. 1995; 92:290.
- [24] Kramida, A., Ralchenko, Yu., Reader, J., and NIST ASD Team (2015). NIST Atomic Spectra Database (ver. 5.3), [Online]. Available: <http://physics.nist.gov/asd>. National Institute of Standards and Technology, Gaithersburg, MD.
- [25] Ludlow J. A., Lee T. G., Ballance C. P., Loch S. D., and Pindzola M. S., Phys. Rev. A 2011; 84:022701.
- [26] Malespin C., Ballance C. P., Pindzola M. S., Witthoef M. C., Kallman T. R. and Loch S. D., A&A 2011, 526:A115.
- [27] McLaughlin B M and Bell K L, J. Phys. B: At. Mol. Opt. Phys. 2000; 33:597.
- [28] McLaughlin B M, Daw A and Bell K L, J. Phys. B: At. Mol. Opt. Phys. 2002; 35:283.
- [29] McLaughlin B. M., Lee Teck-Ghee, Ludlow J. A., et al, J. Phys. B 2011, 44:175206.
- [30] Meijerink R., Glassgold A. E. and Najita J. R., APJ 2008; 676:518.
- [31] Munoz Burgos J. M., Loch S. D., Ballance C. P., and Boivin R. F., A&A 2009; 500:1253.
- [32] Munoz Burgos J. M., Loch S. D., Ballance C. P., and Boivin R. F., A&A 2009; 500:1253.
- [33] Norrington P H and Grant I P, J. Phys. B: At. Mol. Phys 1981; 14:L261.
- [34] Parpia, F., Froese-Fischer, C., and Grant, I. P.: *Comput. Phys. Commun.* **94** 249 (2006)
- [35] Bahcall J. N. and Wolf R. A., ApJ 1968, 152: 701
- [36] Pradhan A. K., J. Phys. B: At. Mol. Phys. 1974; 17:L503.
- [37] Saraph H. E. and Tully J. A., Astron. Astrophys. Suppl. 1994; 107:29
- [38] Seaton M J, Proc. R. Soc. A 1953; 218:400.
- [39] Witthoef M C, Whiteford A D and Badnell N. R., J. Phys. B: At. Mol. Phys 2007; 40:2969.
- [40] Wu Di, Loch S. D., Pindzola M. S., and Ballance C. P., Phys. Rev. A 2012; 85:012711.
- [41] *R-matrix DARC and BP codes website* <http://conorb.freeshell.org>

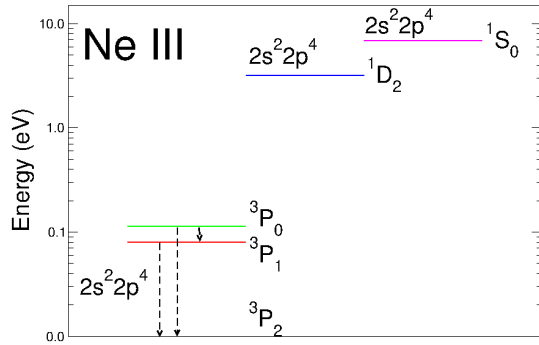


FIG. 1: Energy diagram for  $\text{Ne}^{2+}$ . Three transitions are shown:  $2s^2 2p^4 (^3P_1) - (^3P_2)$ ,  $2s^2 2p^4 (^3P_0) - (^3P_1)$ , and  $2s^2 2p^4 (^3P_0) - (^3P_2)$ .

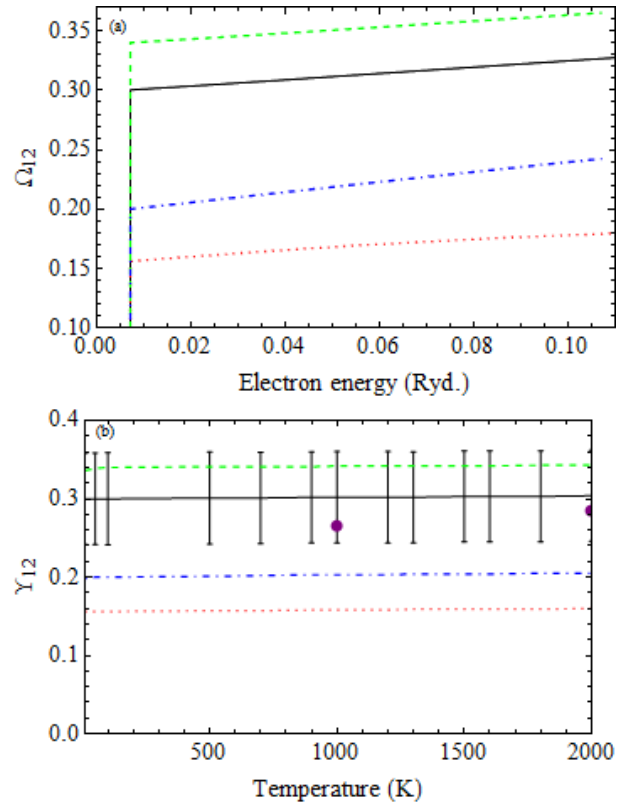


FIG. 2: Comparison of  $\text{Ne}^+$  collision strengths (a) and effective collision strengths (b) for the  $2s^2 2p^5 (^2P_{3/2}^0) - (^2P_{1/2}^0)$  transition between different target expansions: DARC  $n = 2$  (black solid line), DARC  $n = 3$  (red dotted line), BP  $n = 2$  (green dashed line), and BP  $n = 3$  (blue dot-dashed line). Uncertainty estimates are given for our recommended DARC  $n = 2$  results with comparison to the previous  $R$ -matrix calculation (purple circles) of Griffin et al. (2001).

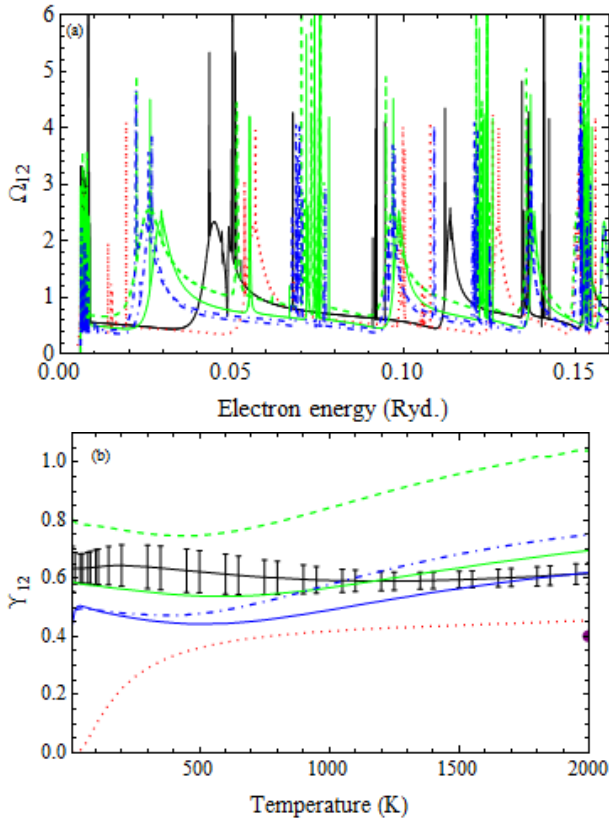


FIG. 3: Comparison of  $\text{Ne}^{2+}$  collision strengths (a) and effective collision strengths (b) for the  $2s^22p^4$  ( $^3P_2$ ) - ( $^3P_1$ ) transition between different target expansions: DARC  $n = 2$  (black solid line), DARC  $n = 3$  (red dotted line), BP  $n = 2$  (green dashed line), BP  $n = 3$  (blue dot-dashed line), BP(op)  $n = 2$  (green solid line), BP(op)  $n = 3$  (blue solid line), and ICFT(op)  $n = 3$  (thick black solid). Uncertainty estimates are given for our recommended DARC  $n = 2$  results with comparison to the previous  $R$ -matrix calculation (purple circle) of McLaughlin et al. (2011).



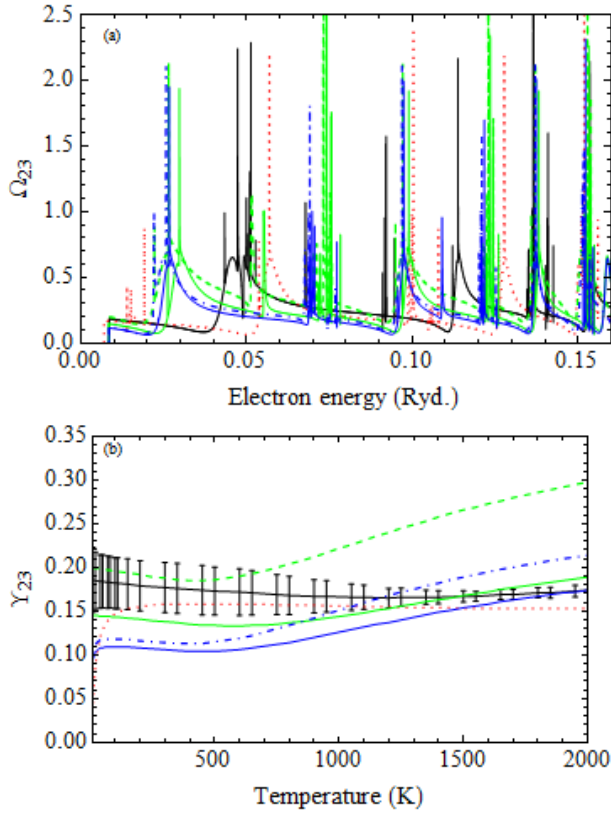


FIG. 4: Comparison of  $\text{Ne}^{2+}$  collision strengths (a) and effective collision strengths (b) for the  $2s^22p^4$  ( $^3P_1$ ) - ( $^3P_0$ ) transition between different target expansions: DARC  $n = 2$  (black solid line), DARC  $n = 3$  (red dotted line), BP  $n = 2$  (green dashed line), BP  $n = 3$  (blue dot-dashed line), BP(op)  $n = 2$  (green solid line), BP(op)  $n = 3$  (blue solid line), and ICFT(op)  $n = 3$  (thick black solid). Uncertainty estimates are given for our recommended DARC  $n = 2$  results.

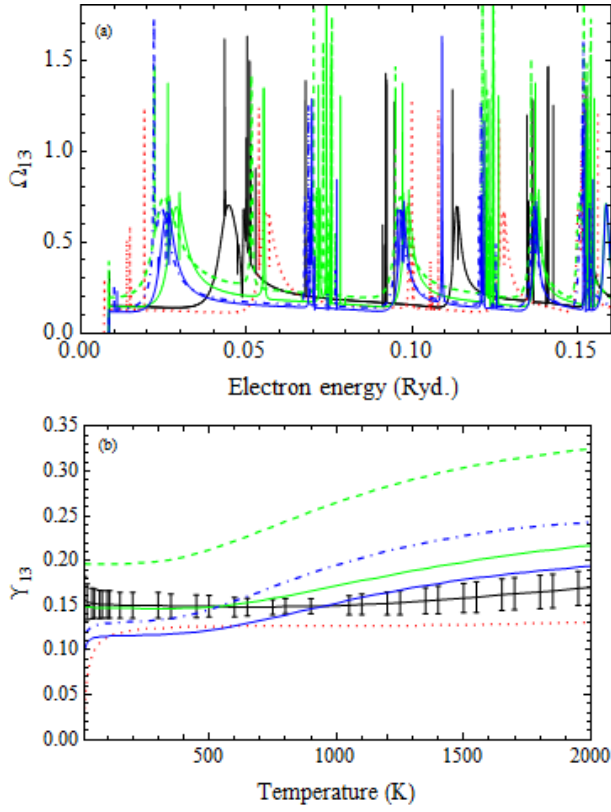


FIG. 5: Comparison of  $\text{Ne}^{2+}$  collision strengths (a) and effective collision strengths (b) for the  $2s^2 2p^4 ({}^3P_2) - ({}^3P_0)$  transition between different target expansions: DARC  $n = 2$  (black solid line), DARC  $n = 3$  (red dotted line), BP  $n = 2$  (green dashed line), BP  $n = 3$  (blue dot-dashed line), BP(op)  $n = 2$  (green solid line), and BP(op)  $n = 3$  (blue solid line). Uncertainty estimates are given for our recommended DARC  $n = 2$  results.

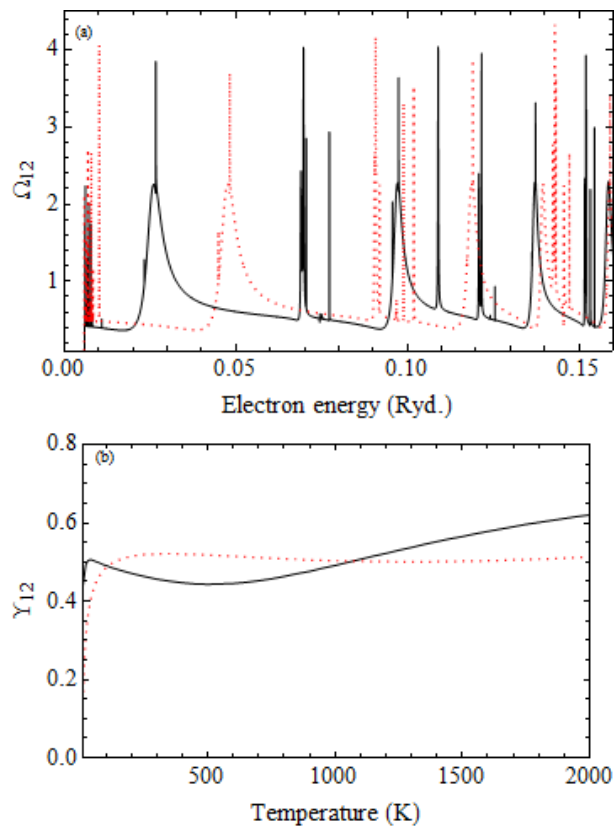


FIG. 6: Comparison of  $\text{Ne}^{2+}$  collision strengths (top) and effective collision strengths (bottom) for the  $2s^22p^4$  ( $^3P_2$ ) - ( $^3P_1$ ) transition: BP(op)  $n = 3$  with (black solid line) and without (red dotted line) the energy shift.

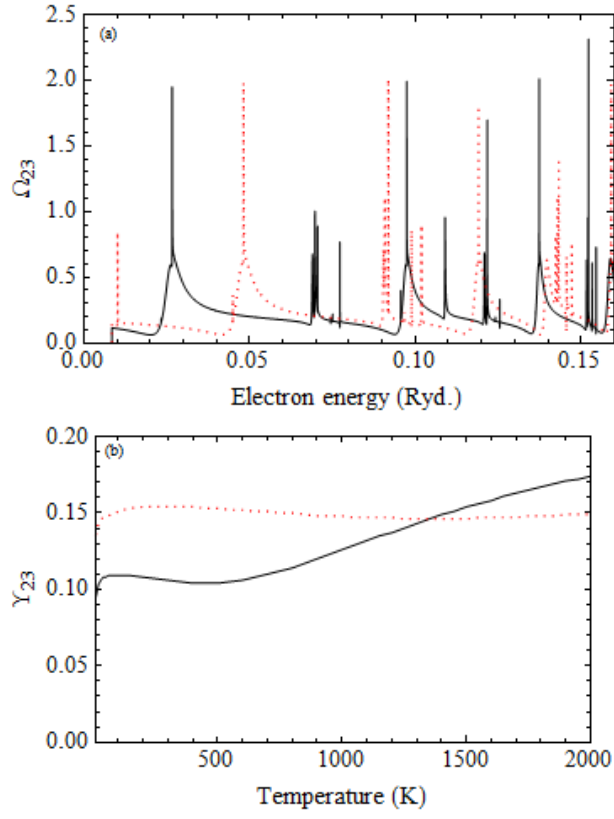


FIG. 7: Comparison of  $\text{Ne}^{2+}$  collision strengths (top) and effective collision strengths (bottom) for the  $2s^22p^4$  ( $^3P_1$ ) - ( $^3P_0$ ) transition: BP(op)  $n = 3$  with (black solid line) and without (red dotted line) the energy shift.

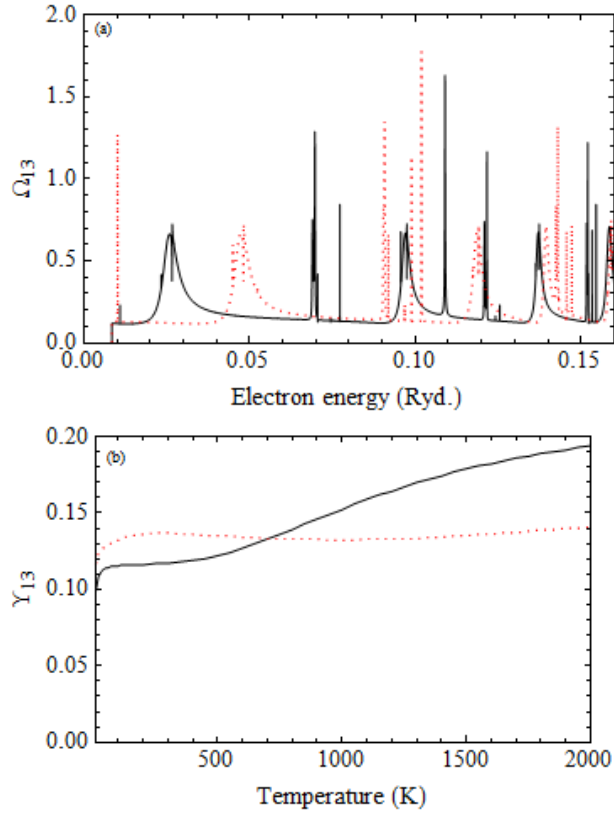


FIG. 8: Comparison of  $\text{Ne}^{2+}$  collision strengths (top) and effective collision strengths (bottom) for the  $2s^22p^4$  ( $^3P_2$ ) - ( $^3P_0$ ) transition: BP(op)  $n = 3$  with (black solid line) and without (red dotted line) the energy shift.

Ne <sup>+</sup> DARC/BP $n = 2$	Ne <sup>+</sup> DARC/BP $n = 3$	Ne <sup>2+</sup> DARC/BP $n = 2$	Ne <sup>2+</sup> DARC/BP $n = 3$
1s <sup>2</sup> 2s <sup>2</sup> 2p <sup>5</sup> 1s <sup>2</sup> 2s2p <sup>6</sup>	1s <sup>2</sup> 2s <sup>2</sup> 2p <sup>5</sup> 1s <sup>2</sup> 2s2p <sup>6</sup> 1s <sup>2</sup> 2s2p <sup>5</sup> 3l 1s <sup>2</sup> 2s <sup>2</sup> 2p <sup>4</sup> 3l	1s <sup>2</sup> 2s <sup>2</sup> 2p <sup>4</sup> 1s <sup>2</sup> 2p <sup>6</sup> 1s <sup>2</sup> 2s2p <sup>5</sup>	1s <sup>2</sup> 2s <sup>2</sup> 2p <sup>4</sup> 1s <sup>2</sup> 2p <sup>6</sup> 1s <sup>2</sup> 2s2p <sup>5</sup> 1s <sup>2</sup> 2s2p <sup>4</sup> 3l 1s <sup>2</sup> 2s <sup>2</sup> 2p <sup>3</sup> 3l 1s <sup>2</sup> 2p <sup>5</sup> 3l

TABLE I: Target expansions for Ne<sup>+</sup> and Ne<sup>2+</sup>.

	Ne <sup>+</sup> $n = 2$ DARC, BP	Ne <sup>+</sup> $n = 3$ DARC, BP	Ne <sup>2+</sup> $n = 2$ DARC, BP	Ne <sup>2+</sup> $n = 3$ DARC, BP
Radius of $R$ -matrix sphere (a.u.)	5.40, 5.87	19.83, 21.60	4.89, 5.24	13.28, 14.35
Continuum basis orbitals for each angular momentum	20	20	20	20
Partial waves $J$	0 – 20	0 – 20	0 – 20	0 – 20
Energy mesh (Ryd.)	$2.5 \times 10^{-6}$	$2.5 \times 10^{-6}$	$3.125 \times 10^{-6}$	$3.125 \times 10^{-6}$
Energy range (Ryd.)	0.007 – 0.107	0.007 – 0.107	0.0058 – 0.1658	0.0058 – 0.1658
Temperature range (K)	10 – 2000	10 – 2000	10 – 2000	10 – 2000

TABLE II: Scattering calculation parameters for different target expansions.

Configuration	Term ( $^{2s+1}L_J$ )	NIST	BP $n = 2$	Err(%)	BP $n = 3$	Err(%)	DARC $n = 2$	Err(%)	DARC $n = 3$	Err(%)
2s <sup>2</sup> 2p <sup>5</sup>	<sup>2</sup> P <sub>3/2</sub> <sup>0</sup>	0.0000	0.0000	0	0.0000	0	0.0000	0	0.0000	0
	<sup>2</sup> P <sub>1/2</sub> <sup>0</sup>	0.0071	0.0069	2.82	0.0070	1.91	0.0076	7.2	0.0071	0.84
Avg. err (%)				1.41		0.96		3.6		0.42
2s <sup>2</sup> 2p <sup>4</sup>	<sup>3</sup> P <sub>2</sub>	0.0000	0.0000	0	0.0000	0	0.0000	0	0.0000	0
	<sup>3</sup> P <sub>1</sub>	0.0059	0.0049	15.75	0.0051	13.01	0.0060	1.59	0.0057	3.11
	<sup>3</sup> P <sub>0</sub>	0.0084	0.0073	13.29	0.0075	10.47	0.0088	4.33	0.0084	0.32
	<sup>1</sup> D <sub>2</sub>	0.2355	0.2348	0.27	0.2454	4.23	0.2521	7.05	0.2664	13.15
	<sup>1</sup> S <sub>0</sub>	0.5081	0.4504	11.36	0.4722	7.06	0.4795	5.62	0.5083	0.05
Avg. err (%)				8.13		6.95		3.72		3.33
			BP(op) $n = 2$		BP(op) $n = 3$					
2s <sup>2</sup> 2p <sup>4</sup>	<sup>3</sup> P <sub>2</sub>	0.0000	0.0000	0.00	0.0000	0.00				
	<sup>3</sup> P <sub>1</sub>	0.0059	0.0058	1.47	0.0057	2.64				
	<sup>3</sup> P <sub>0</sub>	0.0084	0.0085	1.22	0.0084	0.05				
	<sup>1</sup> D <sub>2</sub>	0.2355	0.2532	7.52	0.2573	9.25				
	<sup>1</sup> S <sub>0</sub>	0.5081	0.4751	6.48	0.4874	4.07				
Avg. err (%)				3.34		3.20				

TABLE III: Energy comparison of Ne<sup>+</sup> and Ne<sup>2+</sup> (in Ryd). The configurations and terms listed in the first two columns label different levels. The third column gives the corresponding energies from NIST (Kramida et al. 2015). The percent error after each theoretical energy indicates the deviation of the theoretical value from the NIST one. The last line of each table is the average error of each theoretical calculation.

Ion	Transition	NIST	BP $n = 2$	Err(%)	BP $n = 3$	Err(%)	DARC $n = 2$	Err(%)	DARC $n = 3$	Err(%)
Ne <sup>+</sup>	2s <sup>2</sup> 2p <sup>5</sup> ( <sup>2</sup> P <sub>3/2</sub> <sup>0</sup> ) - ( <sup>2</sup> P <sub>1/2</sub> <sup>0</sup> )	8.59e-3	7.84e-3	8.68	8.07e-3	6.1	8.16e-3	5.01	6.22e-3	27.64
Ne <sup>2+</sup>	2s <sup>2</sup> 2p <sup>4</sup> ( <sup>3</sup> P <sub>2</sub> ) - ( <sup>3</sup> P <sub>1</sub> )	5.84e-3	3.57e-3	38.85	3.93e-3	32.7	5.86e-3	0.42	5.11e-3	12.56
	2s <sup>2</sup> 2p <sup>4</sup> ( <sup>3</sup> P <sub>1</sub> ) - ( <sup>3</sup> P <sub>0</sub> )	1.10e-3	9.10e-4	17.2	1.00e-3	8.8	1.15e-3	4.95	9.75e-4	11.37
			BP(op) $n = 2$	Err(%)	BP(op) $n = 3$	Err(%)				
Ne <sup>2+</sup>	2s <sup>2</sup> 2p <sup>4</sup> <sup>3</sup> P <sub>2</sub> - <sup>3</sup> P <sub>1</sub>	5.84e-3	5.71e-3	2.19	5.51e-3	5.63				
	2s <sup>2</sup> 2p <sup>4</sup> <sup>3</sup> P <sub>1</sub> - <sup>3</sup> P <sub>0</sub>	1.10e-3	1.43e-3	30.2	1.39e-3	25.99				

TABLE IV: Einstein A coefficient (in s<sup>-1</sup>) comparison for Ne<sup>+</sup> and Ne<sup>2+</sup> with NIST data. Columns as in Table II.

Temperature (K)	Ne <sup>+</sup> 2s <sup>2</sup> 2p <sup>5</sup> ( <sup>2</sup> P <sub>3/2</sub> <sup>o</sup> ) - ( <sup>2</sup> P <sub>1/2</sub> <sup>o</sup> ) Υ <sub>12</sub> , %Δ, q <sub>12</sub> (cm <sup>-3</sup> )	Ne <sup>2+</sup> 2s <sup>2</sup> 2p <sup>4</sup> ( <sup>3</sup> P <sub>2</sub> ) - ( <sup>3</sup> P <sub>1</sub> ) Υ <sub>12</sub> , %Δ, q <sub>12</sub> (cm <sup>-3</sup> )	Ne <sup>2+</sup> 2s <sup>2</sup> 2p <sup>4</sup> ( <sup>3</sup> P <sub>1</sub> ) - ( <sup>3</sup> P <sub>0</sub> ) Υ <sub>23</sub> , %Δ, q <sub>23</sub> (cm <sup>-3</sup> )	Ne <sup>2+</sup> 2s <sup>2</sup> 2p <sup>4</sup> ( <sup>3</sup> P <sub>2</sub> ) - ( <sup>3</sup> P <sub>0</sub> ) Υ <sub>13</sub> , %Δ, q <sub>13</sub> (cm <sup>-3</sup> )
1.00×10 <sup>1</sup>	0.30, 4.77, 4.42×10 <sup>-56</sup>	0.63, 12.2, 1.25×10 <sup>-47</sup>	0.19, 19.8, 1.24×10 <sup>-24</sup>	0.16, 16.2, 2.27×10 <sup>-65</sup>
4.00×10 <sup>1</sup>	0.30, 4.78, 6.97×10 <sup>-20</sup>	0.64, 7.73, 1.34×10 <sup>-17</sup>	0.18, 16.7, 4.35×10 <sup>-12</sup>	0.15, 11.2, 1.67×10 <sup>-22</sup>
7.00×10 <sup>1</sup>	0.30, 4.81, 8.63×10 <sup>-15</sup>	0.64, 8.49, 2.19×10 <sup>-13</sup>	0.18, 16.3, 2.24×10 <sup>-10</sup>	0.15, 10.4, 1.85×10 <sup>-16</sup>
1.00×10 <sup>2</sup>	0.30, 4.81, 8.80×10 <sup>-13</sup>	0.64, 9.29, 9.96×10 <sup>-12</sup>	0.18, 16.0, 1.01×10 <sup>-09</sup>	0.15, 10.0, 4.55×10 <sup>-14</sup>
1.50×10 <sup>2</sup>	0.30, 4.80, 3.02×10 <sup>-11</sup>	0.64, 10.3, 1.83×10 <sup>-10</sup>	0.18, 16.0, 3.06×10 <sup>-09</sup>	0.15, 9.62, 3.07×10 <sup>-12</sup>
3.00×10 <sup>2</sup>	0.30, 4.76, 8.95×10 <sup>-10</sup>	0.64, 11.7, 2.86×10 <sup>-09</sup>	0.18, 16.2, 7.89×10 <sup>-09</sup>	0.15, 9.49, 1.80×10 <sup>-10</sup>
4.50×10 <sup>2</sup>	0.30, 4.79, 2.54×10 <sup>-09</sup>	0.63, 11.9, 6.44×10 <sup>-09</sup>	0.17, 16.3, 9.82×10 <sup>-09</sup>	0.15, 8.56, 6.37×10 <sup>-10</sup>
6.00×10 <sup>2</sup>	0.30, 4.75, 4.09×10 <sup>-09</sup>	0.62, 11.2, 9.18×10 <sup>-09</sup>	0.17, 15.5, 1.05×10 <sup>-08</sup>	0.15, 7.21, 1.14×10 <sup>-09</sup>
7.50×10 <sup>2</sup>	0.30, 4.75, 5.34×10 <sup>-09</sup>	0.60, 9.92, 1.10×10 <sup>-08</sup>	0.17, 13.6, 1.05×10 <sup>-08</sup>	0.15, 5.79, 1.59×10 <sup>-09</sup>
9.00×10 <sup>2</sup>	0.30, 4.71, 6.25×10 <sup>-09</sup>	0.60, 8.36, 1.22×10 <sup>-08</sup>	0.17, 11.3, 1.03×10 <sup>-08</sup>	0.15, 5.72, 1.96×10 <sup>-09</sup>
1.05×10 <sup>3</sup>	0.30, 4.74, 6.91×10 <sup>-09</sup>	0.59, 6.75, 1.30×10 <sup>-08</sup>	0.17, 9.11, 1.01×10 <sup>-08</sup>	0.15, 7.10, 2.26×10 <sup>-09</sup>
1.20×10 <sup>3</sup>	0.30, 4.74, 7.39×10 <sup>-09</sup>	0.59, 5.59, 1.35×10 <sup>-08</sup>	0.17, 6.69, 9.86×10 <sup>-09</sup>	0.15, 8.36, 2.51×10 <sup>-09</sup>
1.35×10 <sup>3</sup>	0.30, 4.70, 7.73×10 <sup>-09</sup>	0.59, 4.91, 1.39×10 <sup>-08</sup>	0.17, 4.84, 9.70×10 <sup>-09</sup>	0.16, 9.48, 2.73×10 <sup>-09</sup>
1.50×10 <sup>3</sup>	0.30, 4.70, 7.99×10 <sup>-09</sup>	0.60, 4.75, 1.43×10 <sup>-08</sup>	0.17, 3.82, 9.53×10 <sup>-09</sup>	0.16, 10.3, 2.91×10 <sup>-09</sup>
1.65×10 <sup>3</sup>	0.30, 4.66, 8.16×10 <sup>-09</sup>	0.60, 5.01, 1.45×10 <sup>-08</sup>	0.17, 3.39, 9.42×10 <sup>-09</sup>	0.16, 10.8, 3.08×10 <sup>-09</sup>
1.80×10 <sup>3</sup>	0.30, 4.69, 8.27×10 <sup>-09</sup>	0.61, 5.41, 1.47×10 <sup>-08</sup>	0.17, 3.44, 9.31×10 <sup>-09</sup>	0.17, 11.4, 3.21×10 <sup>-09</sup>
1.95×10 <sup>3</sup>	0.30, 4.69, 8.33×10 <sup>-09</sup>	0.62, 5.75, 1.49×10 <sup>-08</sup>	0.17, 3.81, 9.20×10 <sup>-09</sup>	0.17, 11.4, 3.35×10 <sup>-09</sup>
2.00×10 <sup>3</sup>	0.30, 4.68, 8.37×10 <sup>-09</sup>	0.62, 5.85, 1.49×10 <sup>-08</sup>	0.17, 3.94, 9.19×10 <sup>-09</sup>	0.17, 11.3, 3.38×10 <sup>-09</sup>

TABLE V: Effective collision strengths  $\Upsilon_{12}$ , uncertainty % $\Delta$  and excitation rate coefficients  $q_{ij}$  for Ne<sup>+</sup> and Ne<sup>2+</sup> calculated by the DARC approach with  $n = 2$  target expansion.